

Electronic Supporting Information for:

Role of Crystal Size on Swing-Effect and Adsorption Induced Structure Transition of ZIF-8

Tian Tian,^a Michael T. Wharmby,^b José B. Parra,^c Conchi O. Ania^c and David Fairen-Jimenez^{a,*}

^a*Department of Chemical Engineering & Biotechnology, University of Cambridge, Pembroke Street, Cambridge CB2 3RA, United Kingdom. Email: df334@cam.ac.uk; website: <http://people.ds.cam.ac.uk/df334>*

^b*Diamond Light Source Ltd., Diamond House, Harwell Science & Innovation Campus, Didcot, Oxon., OX11 0DE UK*

^c*Instituto Nacional del Carbón, INCAR-CSIC, Oviedo, Spain*

Contents

S1 Instruments	1
S2 Particle size distribution	2
S3 BET representation	3
S4 N ₂ adsorption/desorption	5
S5 Equilibrium time	7
S6 <i>In situ</i> XRD	8
Sample Preparation	8
Data Collection Details	8
Data Analysis	9
S7 References	24

S1 Instruments

X-ray diffraction (XRD) patterns were recorded with a Bruker D8 diffractometer using CuK α_1 ($\lambda=0.15405$ Å⁻¹) radiation with a step of 0.02° at a scanning speed of 0.1°s⁻¹. Scanning electron microscope (SEM) images were taken by Hitachi S-5500 FE SEM with an accelerating voltage of 5kV without gold coating. N₂ adsorption isotherms were undertaken at 77 K using a Micromeritics ASAP 2020 instrument. Prior to the N₂ adsorption, all samples were evacuated overnight for 24 h at 423 K under vacuum.

S2 Particle size distribution

For each sample, 100 particles were randomly selected to measure the size by using Hitachi S-5500 FE SEM. The size distribution, together with average size and standard deviation (SD) are shown in Figure S1.

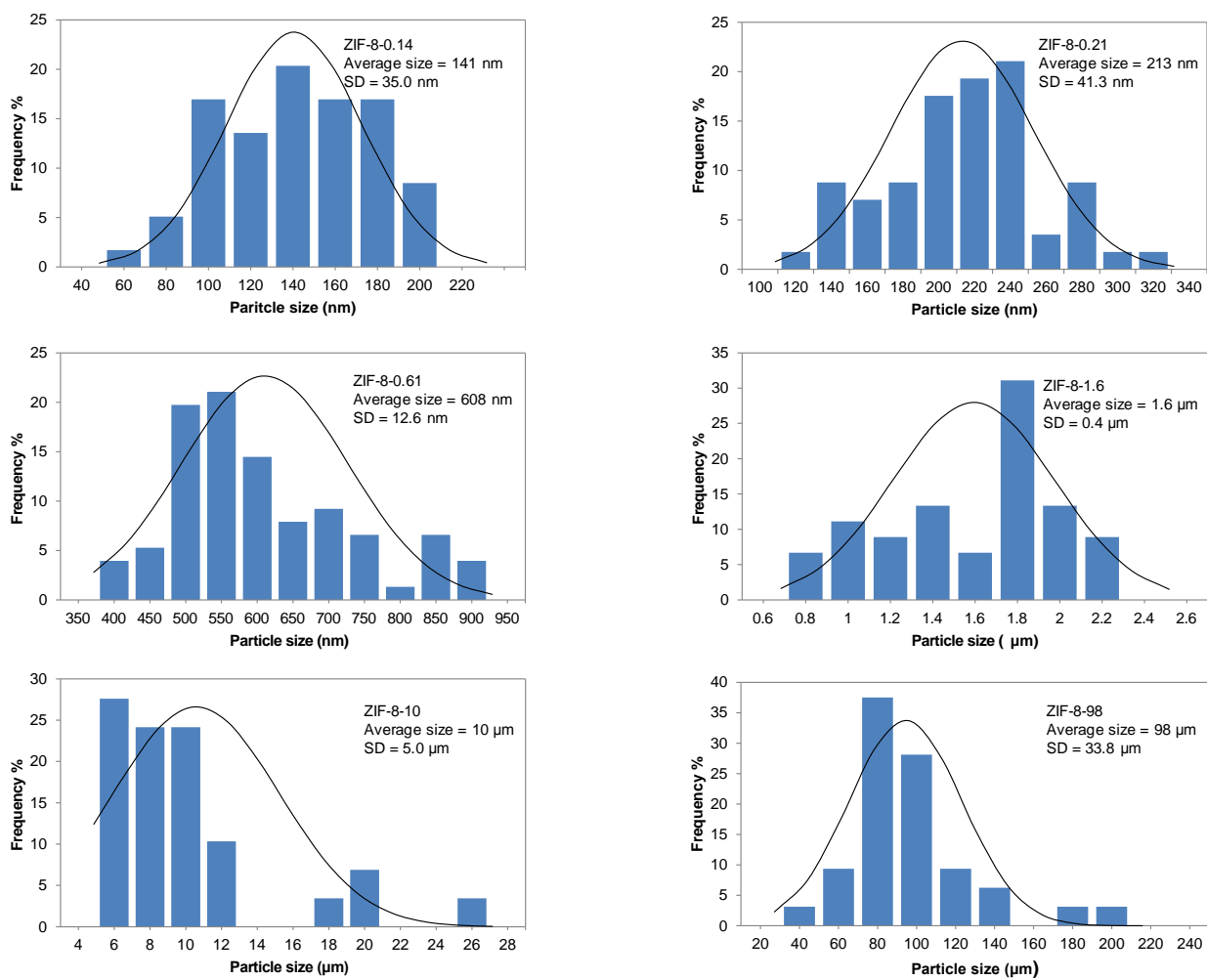


Fig. S1. Size distribution and normal distribution of different ZIF-8 samples.

S3 BET representation

BET area was calculated by Rouquerol's consistency criteria.¹ The plot on left in Fig S2 was used to select the maximum P/P_0 for calculation. The plot on right in Fig S2 was the BET representation by using selected P/P_0 . The plot was not linear due to the phase transition.

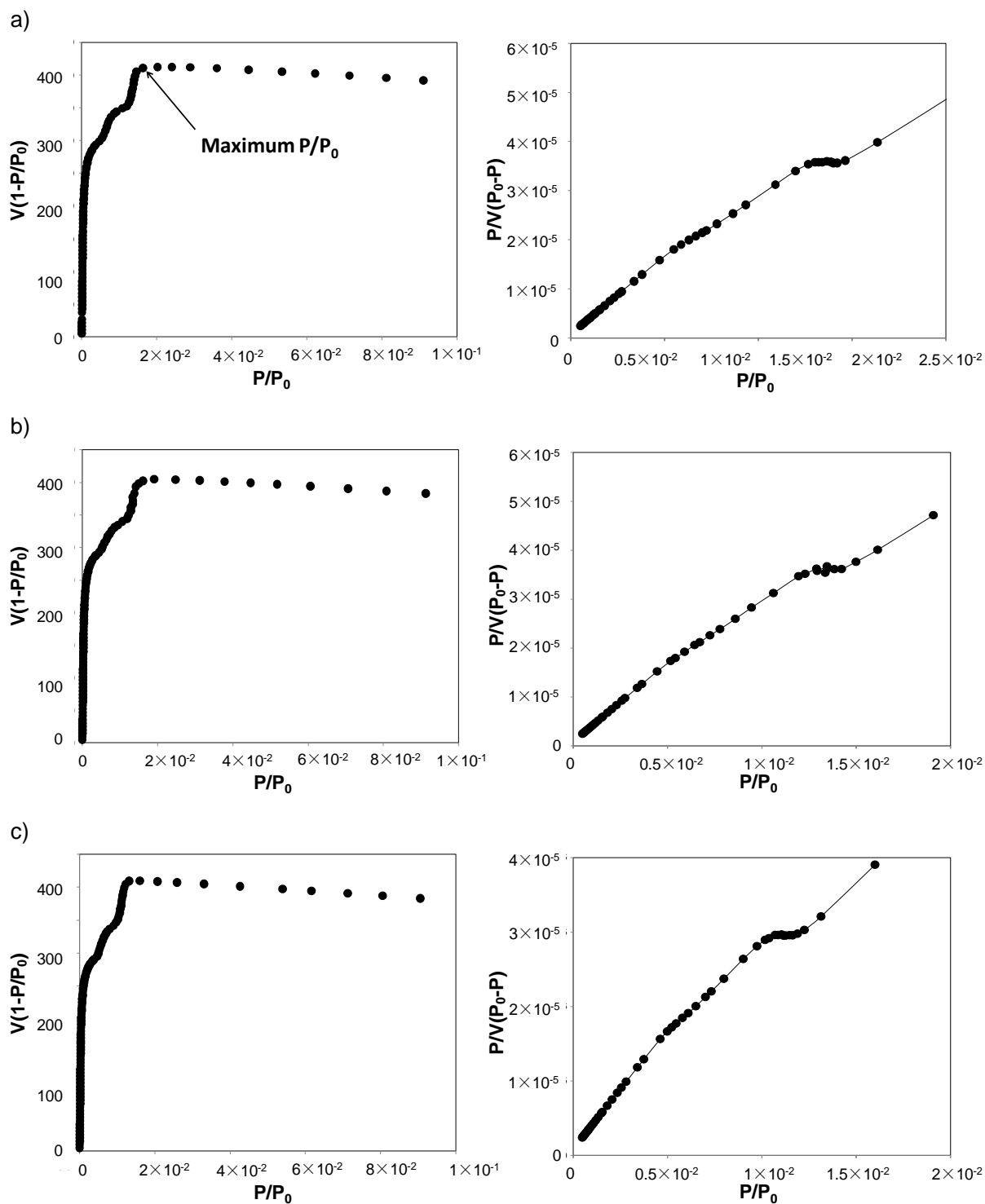


Fig.

S2a. Plot to determine maximum P/P_0 by applying Rouquerol's consistency criteria (*left*) and BET representation of N_2 isotherms (*right*). a) ZIF-8-0.14, b) ZIF-8-0.21, c) ZIF-8-0.61.

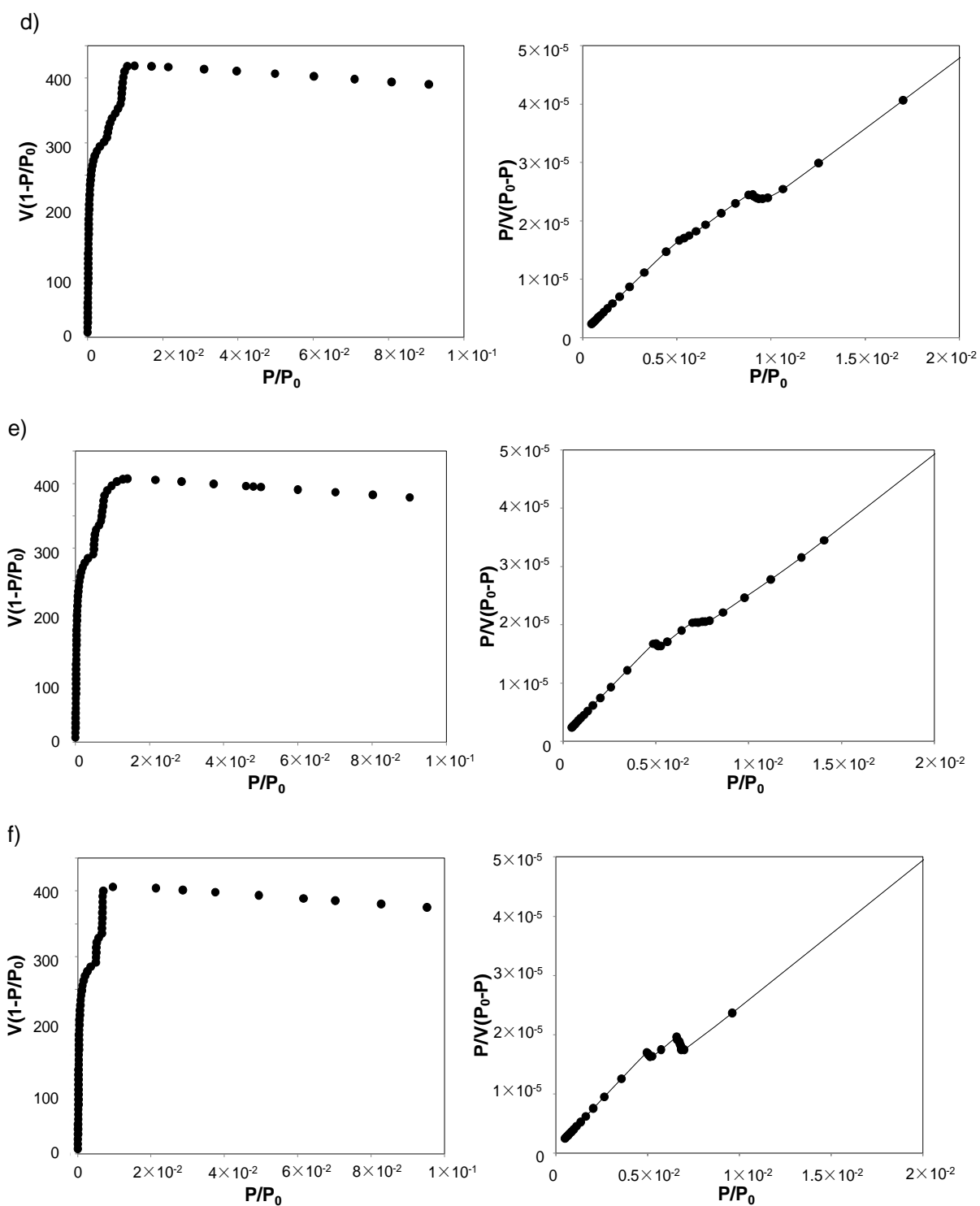


Fig. S2b. Plot to determine maximum P/P_0 by applying Rouquerol's consistency criteria (*left*) and BET representation of N_2 isotherms (*right*). **d)** ZIF-8-1.6, **e)** ZIF-8-10, **f)** ZIF-8-98.

S4 N₂ adsorption/desorption

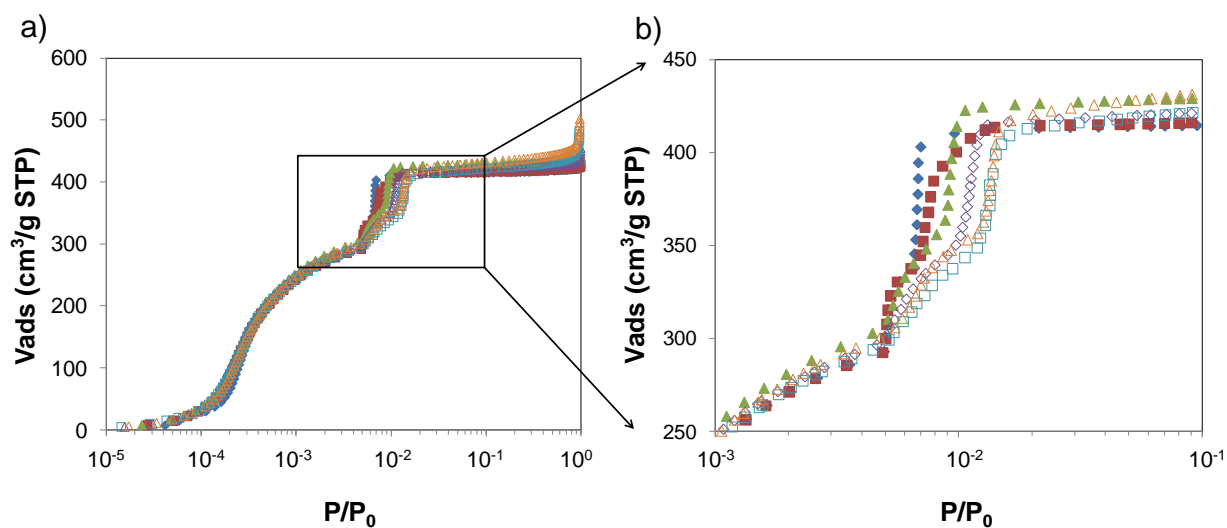


Fig. S3. a) Semi-log plot of N₂ adsorption isotherms at 77 K in ZIF-8 samples with different particle size. Blue closed diamonds, ZIF-98; red closed squares, ZIF-8-10; green closed triangles, ZIF-8-1.6; purple open diamonds, ZIF-8-0.61; blue open squares, ZIF-8-0.21; orange open triangles, ZIF-8-0.14. b) Detail of the N₂ adsorption isotherms plot in the phase transition region.

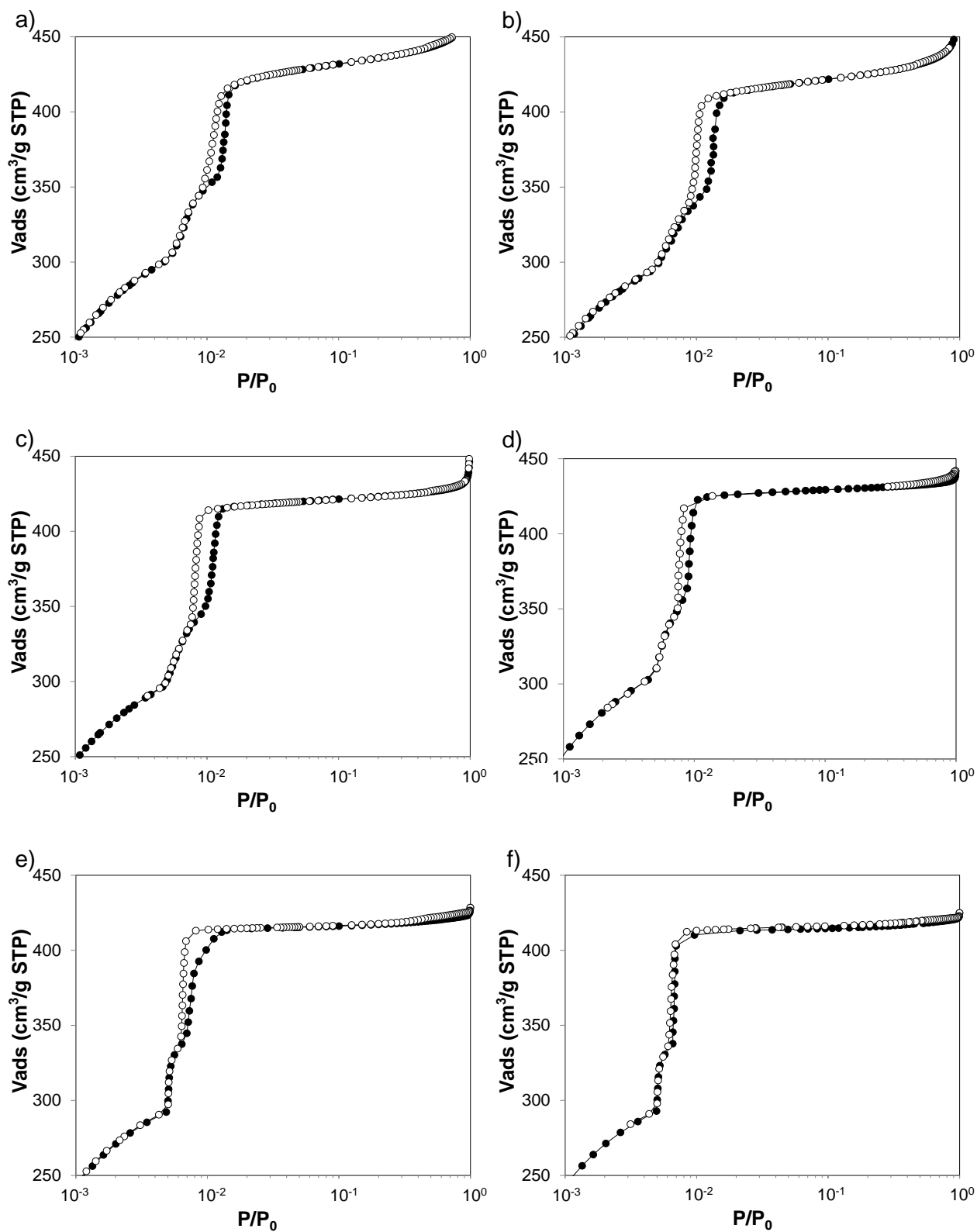


Fig. S4. N₂ adsorption and desorption of ZIF-8 with different particle sizes. **a)** ZIF-8-0.14, **b)** ZIF-8-0.21, **c)** ZIF-8-0.61, **d)** ZIF-8-1.6, **e)** ZIF-8-10, **f)** ZIF-8-98. Closed circles, adsorption; open circles, desorption.

S5 Equilibrium time

The adsorption/desorption equilibrium time for all samples was shown in Fig S5. Before the structure opening, the adsorption time was different for different samples due to the different flexibility of the structure, which highly affects the diffusion of the molecules. The adsorption time was significantly increased at the onset pressure for the two stepped adsorption process. This is mainly due to the rearrangement of adsorbed gas and filling of new gas molecules at the 4-ring window. After the structure transition, the equilibrium time was declined due to the easy accessibility for the opened structure. The same trend was observed for desorption process. The equilibrium time was increased at the threshold pressure for hysteresis loop due to the structure transition and rearrangement of the remaining gases.²

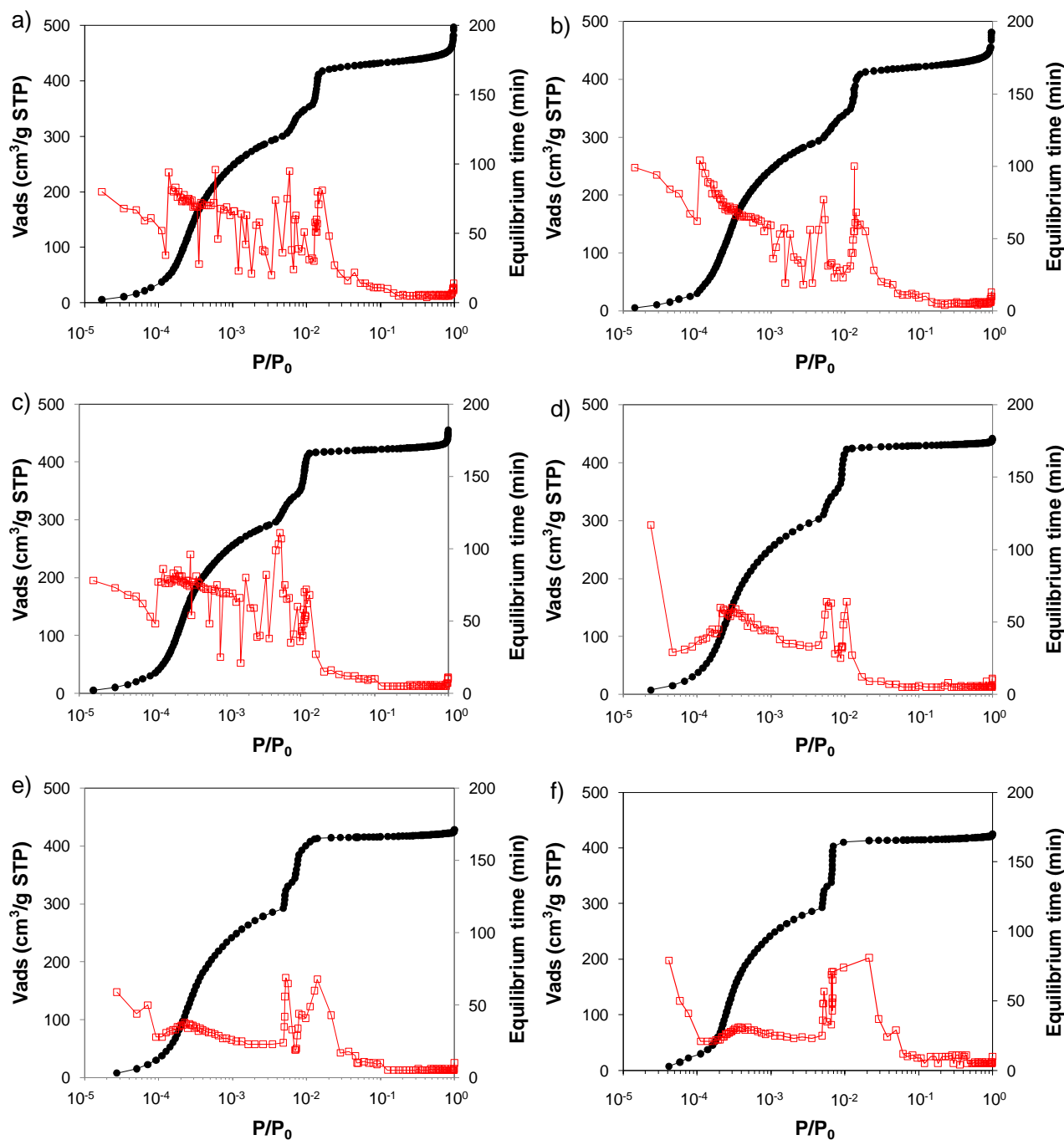


Fig. S5. N₂ adsorption along with equilibrium time for a) ZIF-8-0.14, b) ZIF-8-0.21, c) ZIF-8-0.61, d) ZIF-8-1.6, e) ZIF-8-10, f) ZIF-8-98. Black closed circle, adsorption; red open square, adsorption equilibrium time.

S6 *In situ* XRD

Sample Preparation

ZIF-8-0.14

ZIF-8-0.14, already in the form of a fine powder, was ground in a pestle and mortar to ensure the sample was fully homogenous. The powder was then loaded into a 0.5 mm quartz glass capillary and secured in place by packing a small ball of glass wool on top of the powder. The capillary was then inserted into a brass sealing stub and sealed in place with epoxy resin. Finally the funnel end of the capillary was snapped off and the whole assembly was secured by a Swagelok® fitting in to the I11 gas cell.^{3,4}

ZIF-8-98

ZIF-8-98 was obtained as large blocky and intergrown crystals. The sample was very gently and briefly ground, to yield a particle size that could be loaded into a capillary. As for the ZIF-8-0.14, the powder was loaded into a 0.5 mm quartz glass capillary and secured in place with a small ball of glass wool. It should be noted that due to the large particle size the packing was significantly less homogenous than normally desirable, however this was necessary to facilitate investigation of the particle size effect on structural responsiveness. After loading, the capillary was inserted into a brass sealing stub and sealed in place with epoxy resin. Finally the funnel end of the capillary was snapped off and the whole assembly was secured by a Swagelok® fitting in to the I11 gas cell.^{3,4}

Data Collection Details

All diffraction patterns in this work were collected using the in-house developed 90° arc position sensitive detector at beamline I11,⁵ collecting 8 partial patterns each at a different δ angle (range $\delta = 2.0^\circ$ - 3.75° ; step size of 0.25°) for 1 sec. Patterns were then summed together to remove the gaps between detector plates. Whilst collecting data, the sample was repeatedly rocked on the θ circle through 30° to provide some powder averaging.

Activation

Both ZIF-8-0.14 and ZIF-8-98 were activated in the same way, first offline for about an hour prior to mounting on the diffractometer using a tube furnace heated to 413 K and under dynamic vacuum provided by a turbomolecular pump ($p \sim 1 \times 10^{-6}$ mbar). The sample was then transferred to the diffractometer on beamline I11 at Diamond Light Source (Oxon., UK)⁶ and a diffraction pattern was collected. The sample was activated again for a further 20 mins using an Oxford cryostream heated to 413 K and the turbomolecular pump of the I11 gas handling system.^{3,4} A second diffraction pattern was collected after activation to check the degree of sample degradation, before the sample was cooled under dynamic vacuum to 80 K, using the cryostream.

In Situ Experiment

Once cooled to 80 K, a diffraction pattern of each sample was collected at a pressure of 0 bar (measured using the I11 gas handling system). N_2 gas was then dosed onto the sample, using the I11 gas handling system. A series of 12 pressure points, approximately equally spaced over the range $p(N_2) = 0.00$ - 0.10 bar ($p/p_0 = 0.00$ - 0.07 ; p_0 taken as 1.3687 at 80 K)⁷ were then collected (Table S1). A second series 10 of points were collected with wider spacing over the range $p(N_2) = 0.10$ - 1.35 ($p/p_0 = 0.07$ - 0.99) (Table S1). At each

pressure point, the N₂ pressure in the sample was allowed to equilibrate for 10 mins and the rate of change of the pressure was then observed. If the rate of change was greater than 0.1 mbar in 20 secs, the sample was allowed to equilibrate for a further 5 mins and the rate of change checked again; this process was repeated until the N₂ pressure stabilised. A diffraction pattern of the sample was then collected using the PSD, as described for the activation procedure.

Table S1. N₂ adsorbate pressures at which diffraction patterns were collected for ZIF-8-0.14 and ZIF-8-98 during the *in situ* adsorption experiment.

ZIF-8-0.14/ bar	ZIF-8-98 / bar
0.0000	0.0000
0.0146	0.0069
0.0191	0.0137
0.0277	0.0196
0.0368	0.0278
0.0474	0.0371
0.0581	0.0469
0.0705	0.0575
0.0794	0.0685
0.0847	0.0798
0.0927	0.0868
0.0994	0.0948
0.1566	0.1015
0.2001	0.1526
0.2506	0.2044
0.3500	0.2544
0.4576	0.3486
0.6364	0.4481
0.8284	0.5921
1.0020	0.8079
1.2473	1.0367
1.3580	1.2612
	1.3486

Data Analysis

Each data set was reprocessed to a data range of 2.0°-55.0° with a bin size of 0.004° 2θ using a bespoke Python script. All indexing, Pawley fitting and Rietveld refinement operations, including parametric Rietveld refinement, were performed using the routines implemented in the TOPAS-Academic v5 suite.⁸ It was possible to index all of the diffraction patterns in this work in the reported cubic space group for ZIF-8, *I4̄3m*.

Initial Rietveld Refinements

The diffraction patterns measured for both samples under vacuum were indexed and Pawley fitted. A Rietveld refinement was then performed, using the background, peak profile and unit cell parameters

determined from the Pawley fit, along with the previously reported activated ZIF-8 structure,^{9,10} as a starting model. To account for the poorer averaging of the ZIF-8-98, additional preferred orientation (spherical harmonic model) terms were included in the refinement. To ensure a chemically sensible result, restraints were applied to the Zn-N, N-C and C-C distances, as well as N...C, C...C and N...N non-bonding distances. A further restraint was applied to ensure the imidazolate ring remained flat. The same set of restraints was used for all Rietveld refinements, including the parametric refinement, and these are summarised in Table S2. Good fits to both sets of data were achieved and refinement quality indicators along with the final refined unit cells are included in Table S3.

Table S2. Restraints applied to the framework during the Rietveld refinement, with a schematic of the imidazolate linker and one Zn atom to show where these restraints are applied.

Restraint	Distance \pm Tolerance / Å	
Zn-N	1.99 ± 0.001	
C1-C1	1.37 ± 0.001	
C1-N1	1.37 ± 0.001	
N1-C2	1.30 ± 0.001	
C2-C3	1.52 ± 0.001	
C1...N1a	2.37 ± 0.005	
C1...C2	2.31 ± 0.005	
N1...N1a	2.25 ± 0.005	
C1, N1, C2, C3 (Dihedral angle)	$0.0^\circ \pm 0.001^\circ$	

In the next stage, diffraction pattern measured at the maximum N_2 pressures for each sample (ZIF-8-0.14: $p(N_2) = 1.3580$ bar, $p/p_0 = 0.992$; ZIF-8-98: $p(N_2) = 1.3486$ bar, $p/p_0 = 0.985$) were analysed. Data were indexed and Pawley fits were performed and the profile and cell parameters from these used as starting points for the Rietveld refinement. The respective structure under vacuum was used as a starting point for the refinement, with the restraint set described applied. The positions of the imidazolate linker were then allowed to refine. Once this stabilised, a Fourier difference map was calculated and on the most likely (highest peak) positions, a N_2 molecule was placed. Each N_2 molecule was described as a rigid body, with two N atoms separated by a distance of 1.098 Å; the position of the molecule was described with a 'fake' atom referred to as the Centre Of Mass (COM), placed half way between the two N atoms. Occupancies and orientation of the each molecule were refined first, followed by the position. If molecule's occupancy tended to 0, it was removed and an alternative Fourier difference peak was chosen as an N_2 molecule. By this sequential process a model of the structure of the adsorbed N_2 molecules was developed. In the final cycles of refinement, occupancy and orientation of the N_2 molecules was fixed and the positions and displacement parameters of the N_2 adsorbates and framework were refined together. Good fits to the data were again obtained and the refinement quality indicators are included in Table S3.

Rietveld Refinements at Intermediate Pressures

To identify structural changes in the samples occurring at intermediate N_2 pressures, diffraction patterns were initially visually inspected for obvious shifts in peak positions. For ZIF-8-0.14, four phases with peaks not consistent with either the evacuated or $p(N_2) = 1.3580$ bar structures were identified, whilst for ZIF-8-98 only three phases were identified. However, it was found that diffraction patterns of ZIF-8-98 measured at $p(N_2) = 0.0798$ and 0.0868 bar contained peaks attributed to either two or three of the other observed phases. Thus, these measurements were discarded in subsequent analysis steps.

Each identified phase was Rietveld refined separately, using the structure nearest in N_2 pressure as a starting point. The framework of each structure was refined using the restraints listed in Table S2 and the

structure of the adsorbates was determined using the method described for the $p/p_0 \sim 1$ structures. In the final cycles of refinement, the framework and adsorbate structures were refined together; the final refinement quality indicators are given in Table S3.

Table S3. List of refinement quality parameters and lattice parameters obtained from the final Rietveld refinements of ZIF-8-0.14 and ZIF-8-98 determined as a function of N₂ adsorbate pressure.

ZIF-8-0.14				
N ₂ Pressure (p/p ₀) / bar (-)	Cell Parameter / Å	R _{wp} / %	R _{Bragg} / %	χ^2
0.0000 (0.000)	16.98205(8)	1.84	2.36	6.708
0.0847 (0.062)	17.03920(10)	2.54	2.34	12.302
0.0927 (0.068)	17.03985(8)	1.68	1.22	5.400
0.4576 (0.334)	17.04902(8)	1.60	1.03	4.858
0.6364 (0.465)	17.06286(7)	1.82	1.17	6.311
1.3580 (0.992)	17.10080(7)	1.62	1.24	5.020
ZIF-8-98				
N ₂ Pressure (p/p ₀) / bar (-)	Cell Parameter / Å	R _{wp} / %	R _{Bragg} / %	χ^2
0.0000 (0.000)	17.00499(6)	5.24	5.03	41.967
0.0371 (0.027)	17.00076(5)	4.09	3.02	26.051
0.0575 (0.042)	17.05138(7)	4.87	5.72	36.244
0.0948 (0.069)	17.11474(6)	4.19	3.53	26.788
1.3486 (0.985)	17.11853(3)	3.13	1.94	15.194

Parametric Rietveld Refinement

The individually refined structures were used to set up a parametric Rietveld refinement; during this refinement, the unit cell parameters and atomic positions of these structures were fixed. Initial models of the structures at pressure between the refined structures were derived from the refined structure bounding the range with the highest pressure (e.g. for ZIF-8-0.14 structures between 0.0146 and 0.0794 bar, the 0.0847 bar structure was used rather than the 0.0000 bar structure). Peak profile, background and displacement parameters were constant across all structures. Lattice parameters of the all the unrefined phases were allowed to refine freely. Framework structure was alternately refined with N₂ molecule orientation and occupancy until the refinement was relatively stable, at which point all were refined together. N₂ molecule occupancy was restrained to be greater than the previous structure's occupancy whilst lower than the subsequent structure's, assuming that as the N₂ pressure increases, so the adsorbed amount also increases. Only in the last cycles of refinement were the thermal parameters also refined. Good fits to the data were obtained for the final cycles of both structures – fit quality indicators, and unit cell parameters from the parametric Rietveld refinement are given in Table S4.

Table S4. Results of parametric Rietveld refinement: fit quality indicators and lattice parameters as a function of pressure.

ZIF-8-0.14				
N ₂ Pressure (p/p ₀) / bar (-)	Cell Parameter / Å	R _{wp} / %	R _{Bragg} / %	χ^2
0.0000 (0.000)	16.98289(4)	2.16	3.13	9.276
0.0146 (0.011)	16.99929(4)	2.06	2.09	8.155
0.0191 (0.014)	16.99929(4)	1.90	1.77	6.884
0.0277 (0.020)	16.99929(4)	1.84	1.59	6.495
0.0368 (0.027)	16.99934(4)	1.80	1.52	6.240
0.0474 (0.035)	17.00051(4)	1.80	1.55	6.254
0.0581 (0.042)	17.00676(4)	1.81	1.62	6.239
0.0705 (0.052)	17.01928(4)	1.78	1.53	6.114
0.0794 (0.058)	17.03359(4)	1.84	1.75	6.436
0.0847 (0.062)	17.03847(4)	1.97	2.24	7.368
0.0927 (0.068)	17.03994(4)	1.80	1.16	6.178
0.0994 (0.073)	17.04100(4)	1.85	1.37	6.502
0.1566 (0.114)	17.03950(4)	2.03	2.07	7.775
0.2001 (0.146)	17.03853(4)	2.23	2.51	9.458
0.2506 (0.183)	17.03873(4)	2.57	3.34	12.440
0.3500 (0.256)	17.04065(4)	2.88	3.68	15.773
0.4576 (0.334)	17.04969(4)	2.35	3.32	10.449
0.6364 (0.465)	17.06290(5)	1.97	1.87	7.342
0.8284 (0.605)	17.07699(4)	2.03	1.70	7.813
1.0020 (0.732)	17.08662(4)	1.92	1.67	7.026
1.2473 (0.911)	17.09597(4)	2.05	2.06	7.980
1.3580 (0.992)	17.10034(4)	2.34	3.35	10.425

ZIF-8-98

N ₂ Pressure (p/p ₀) / bar (-)	Cell Parameter / Å	R _{wp} / %	R _{Bragg} / %	χ ²
0.0000 (0.000)	17.00590(3)	5.52	4.94	46.646
0.0069 (0.005)	17.00492(3)	4.97	7.71	38.502
0.0137 (0.010)	17.00381(3)	3.49	2.83	18.979
0.0196 (0.014)	17.00278(3)	3.61	3.07	20.241
0.0278 (0.020)	17.00229(3)	3.71	3.58	21.777
0.0371 (0.027)	17.00185(3)	4.38	3.59	30.3007
0.0469 (0.034)	17.00507(4)	8.86	7.46	121.668
0.0575 (0.042)	17.05243(3)	4.91	5.61	36.848
0.0685 (0.050)	17.05734(3)	8.61	15.79	114.358
0.0798 (0.058)				
0.0868 (0.063)				
0.0948 (0.069)	17.11437(3)	4.67	5.06	33.355
0.1015 (0.074)	17.11421(3)	3.92	4.16	23.588
0.1526 (0.111)	17.11555(3)	5.03	5.54	38.729
0.2044 (0.149)	17.11558(3)	4.18	3.52	26.982
0.2544 (0.186)	17.11613(3)	3.41	3.66	17.973
0.3486 (0.255)	17.11677(3)	3.62	3.16	20.368
0.4481 (0.327)	17.11731(3)	4.27	3.43	28.233
0.5921 (0.433)	17.11784(3)	3.52	3.53	19.011
0.8079 (0.590)	17.11857(3)	3.49	3.91	19.075
1.0367 (0.757)	17.11895(3)	3.35	2.96	17.386
1.2612 (0.921)	17.11889(3)	3.88	5.39	23.497
1.3486 (0.985)	17.11918(3)	3.53	3.05	19.360

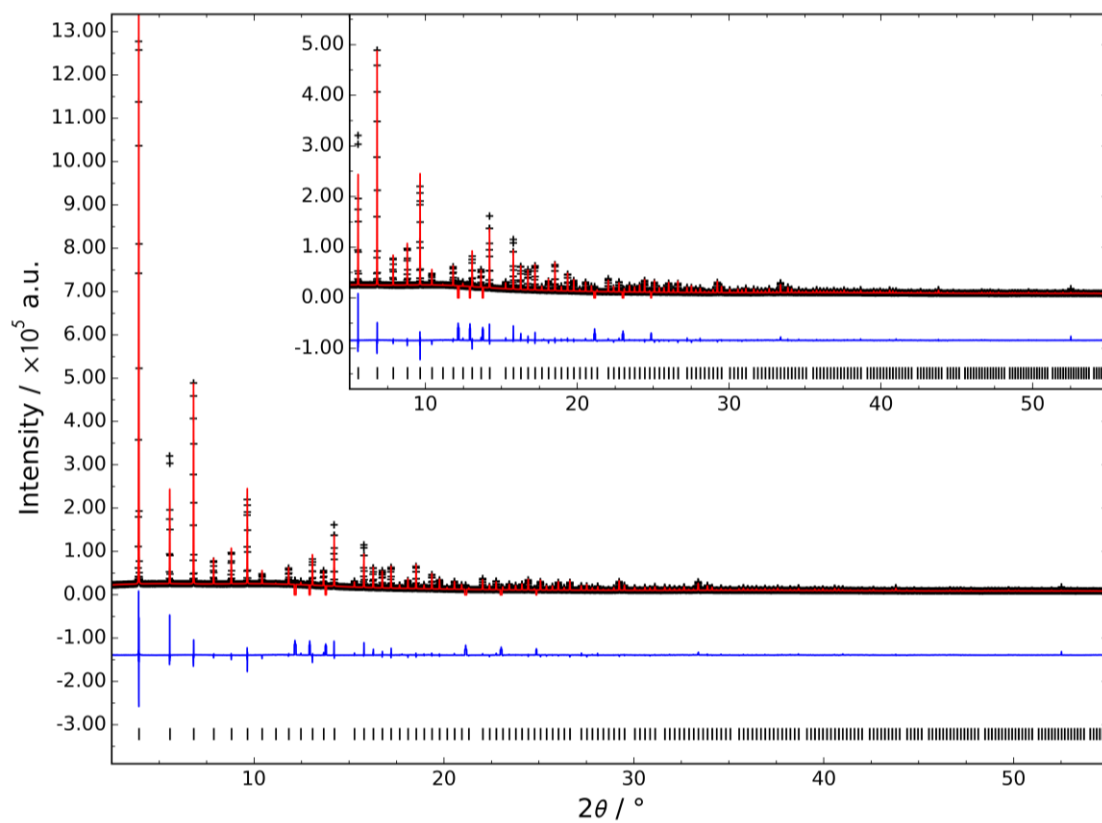
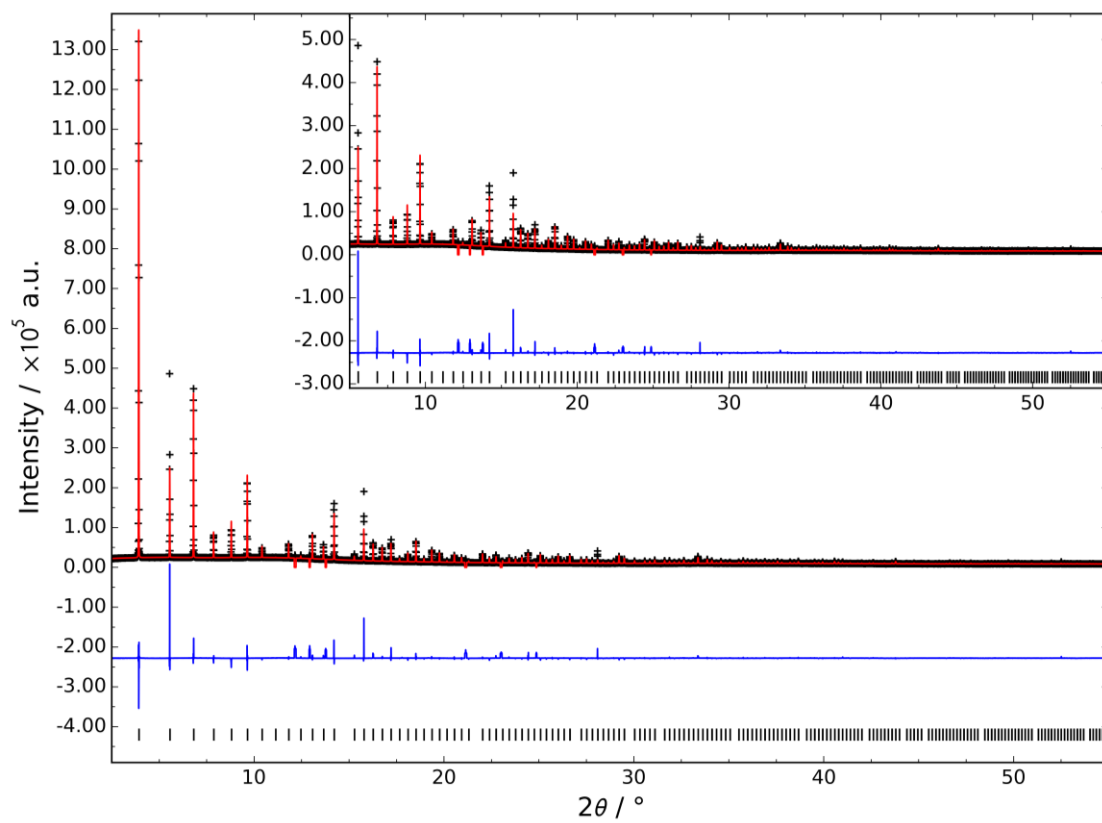


Figure S6a. Observed (black), refined (red), and difference (blue) X-Ray diffraction profiles measured for for **(top)** empty ZIF-8-98, and **(bottom)** ZIF-8-98 loaded with N_2 at 0.0371 bar.

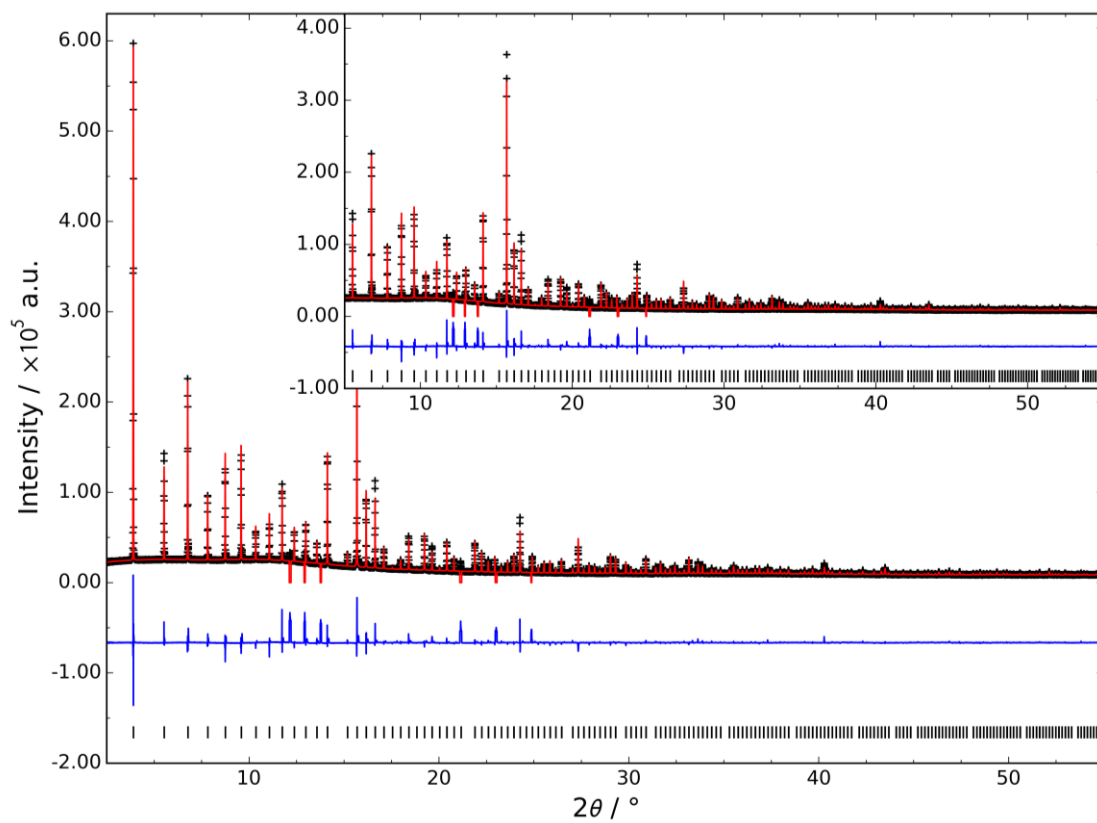
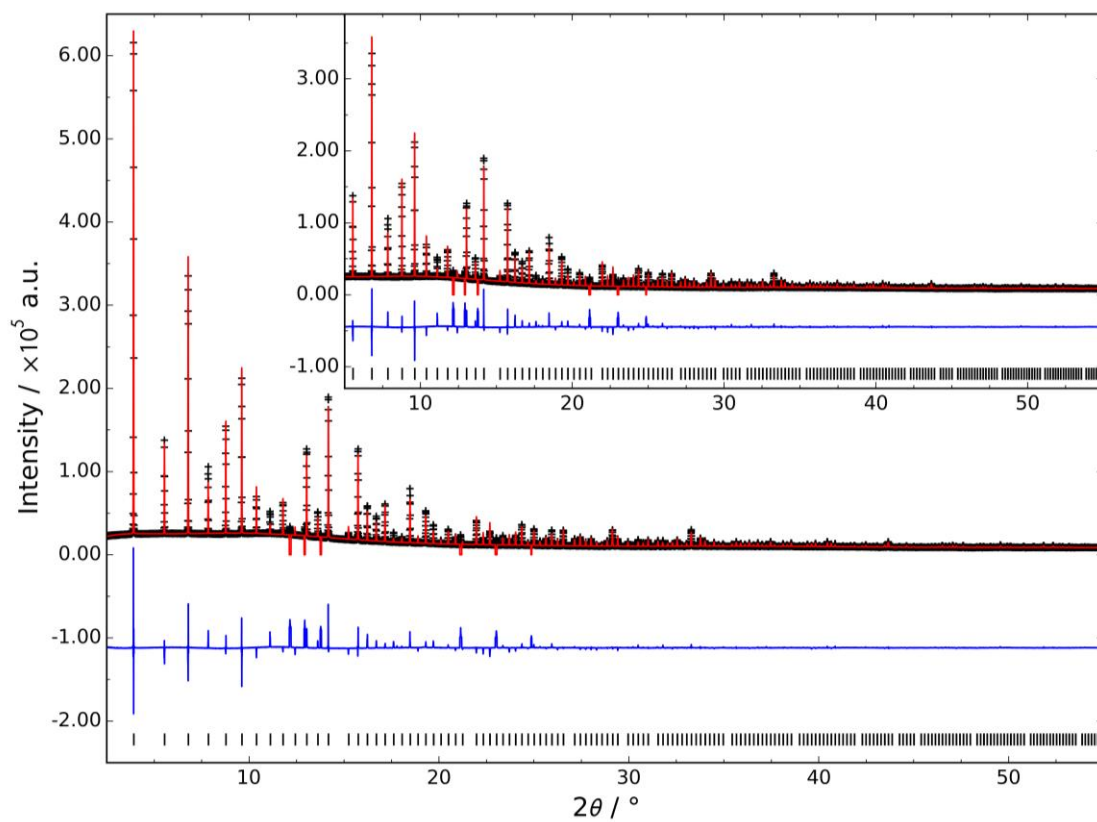


Figure S6b. Observed (black), refined (red), and difference (blue) X-Ray diffraction profiles measured for (top) ZIF-8-98 loaded with N₂ at 0.0575 bar, and (bottom) ZIF-8-98 loaded with N₂ at 0.0948 bar.

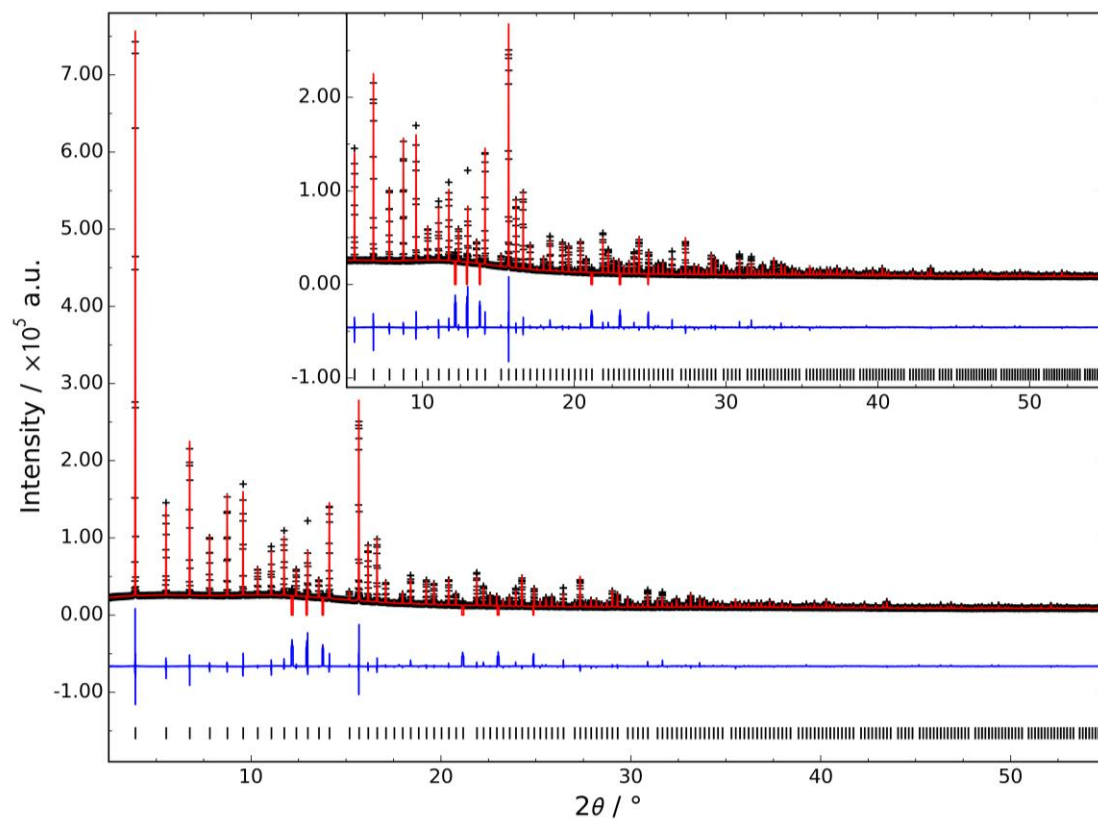


Figure S6c. Observed (black), refined (red), and difference (blue) X-Ray diffraction profiles measured for ZIF-8-98 loaded with N₂ at 1.3486 bar.

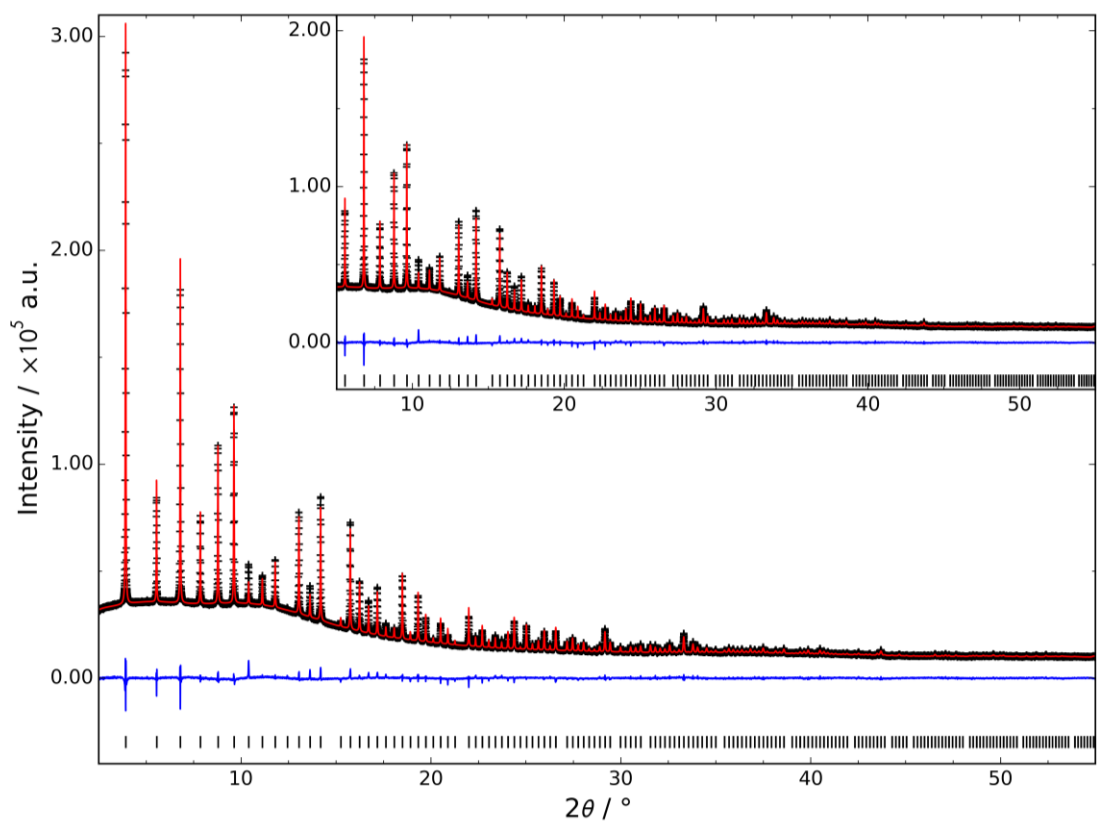
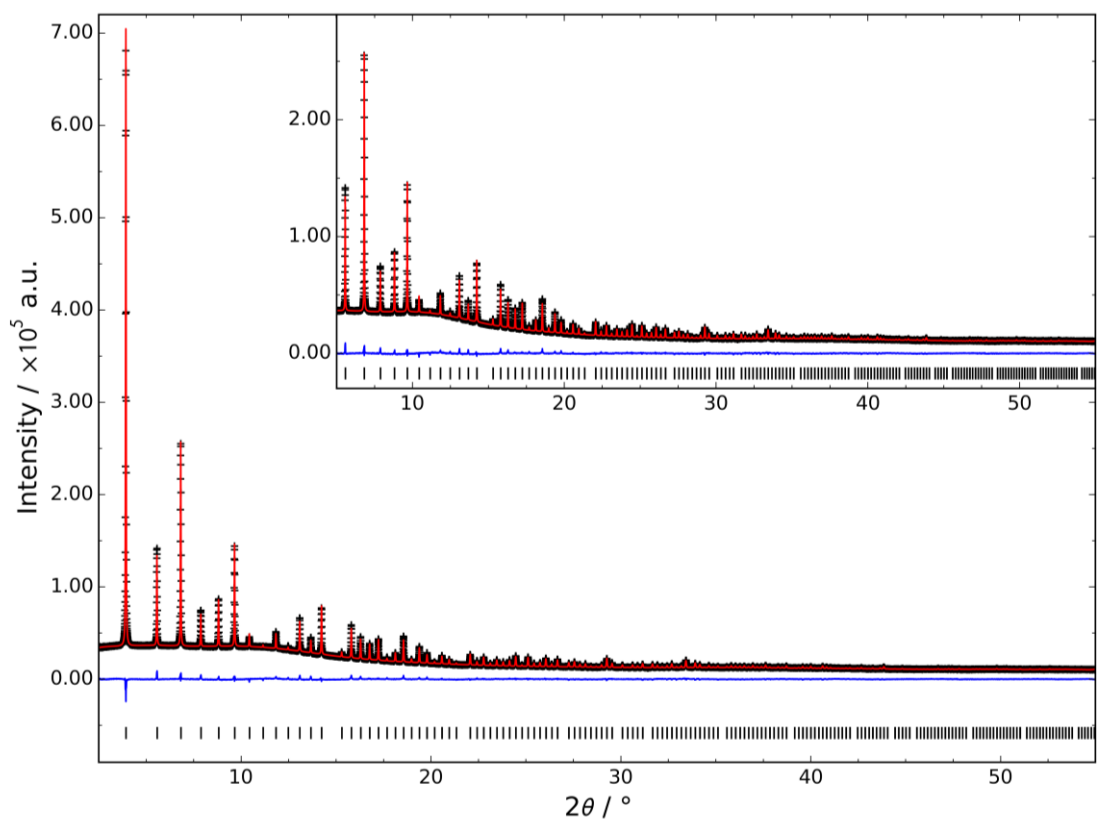


Figure S6d. Observed (black), refined (red), and difference (blue) X-Ray diffraction profiles measured for for **(top)** empty ZIF-8-0.14, and **(bottom)** ZIF-8-0.14 loaded with N_2 at 0.0847 bar.

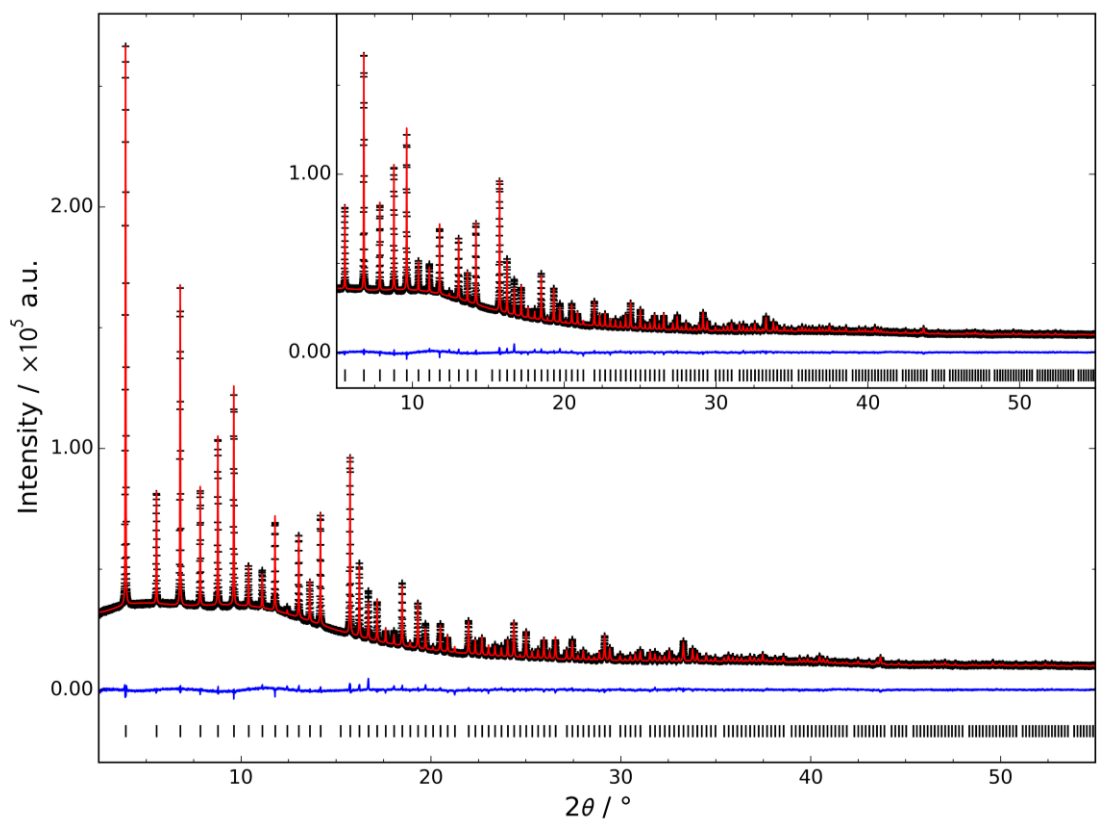
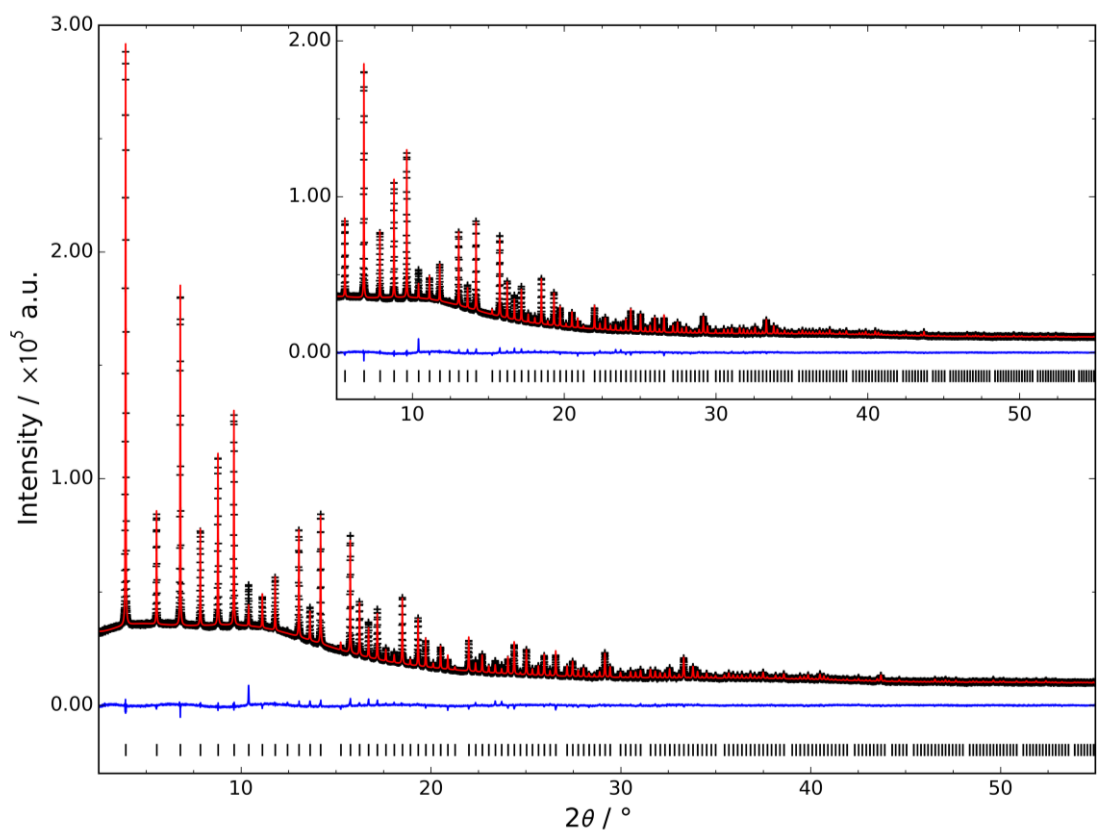


Figure S6e. Observed (black), refined (red), and difference (blue) X-Ray diffraction profiles measured for **(top)** ZIF-8-0.14 loaded with N₂ at 0.0927 bar, and **(bottom)** ZIF-8-0.14 loaded with N₂ at 0.4576 bar.

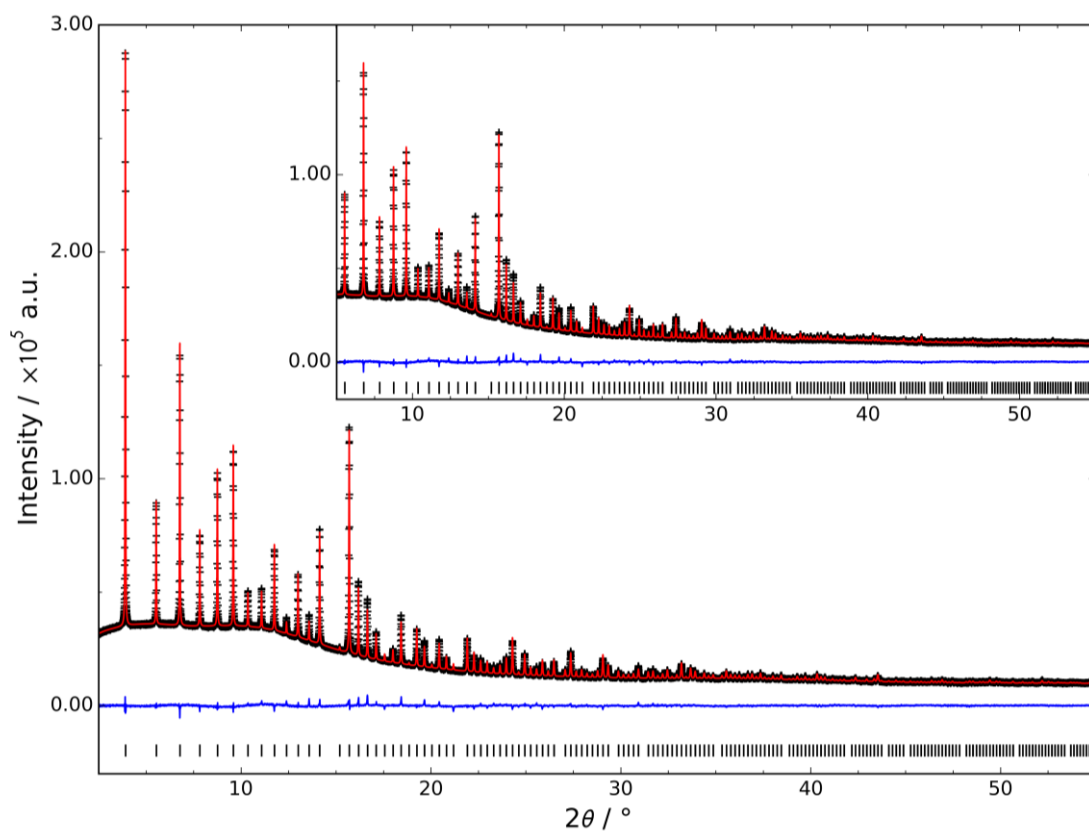
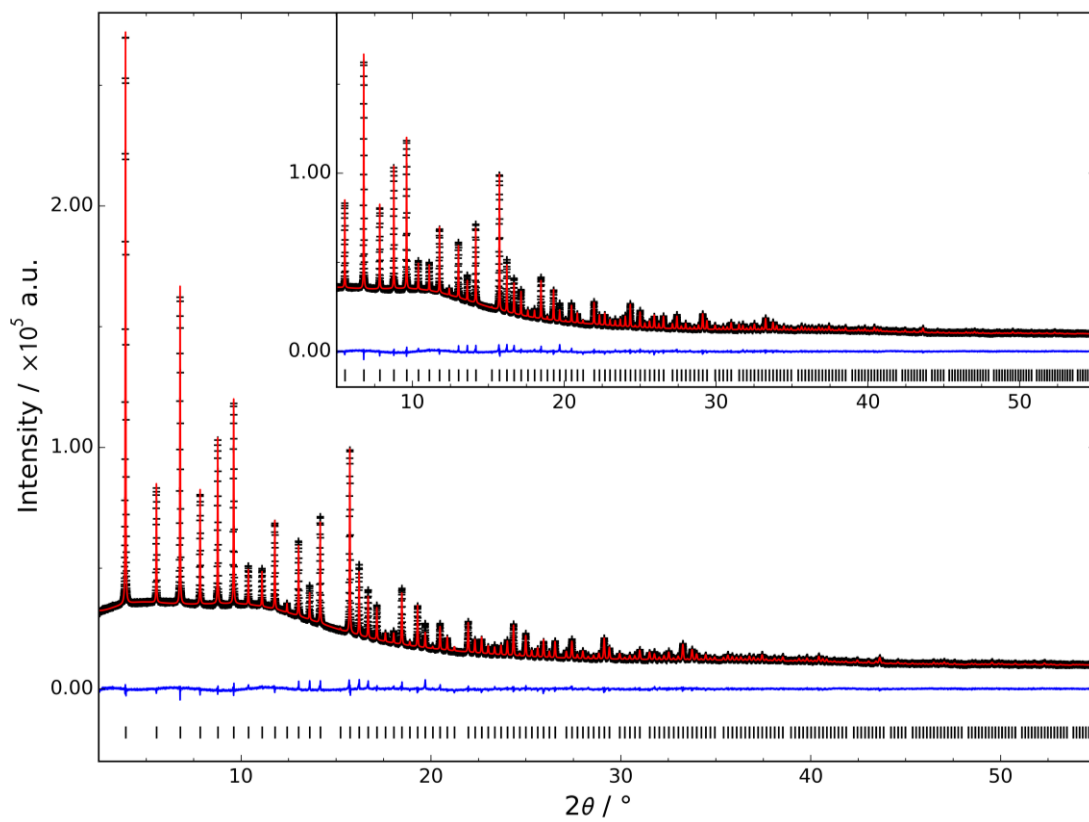


Figure S6f. Observed (black), refined (red), and difference (blue) X-Ray diffraction profiles measured for **(top)** ZIF-8-0.14 loaded with N₂ at 0.6364 bar, and **(bottom)** ZIF-8-0.14 loaded with N₂ at 0.3580 bar.

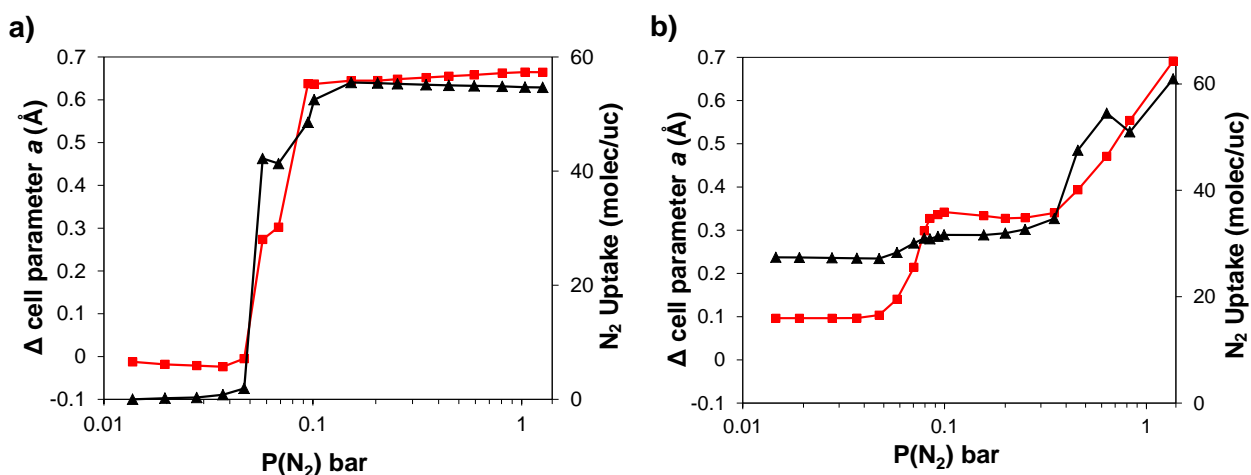


Fig. S7. Change in a cell parameters (red squares) along with the amount of adsorbed N_2 molecules (black triangles) at different $p(N_2)$ for **a)** ZIF-8-98 and **b)** ZIF-8-0.14.

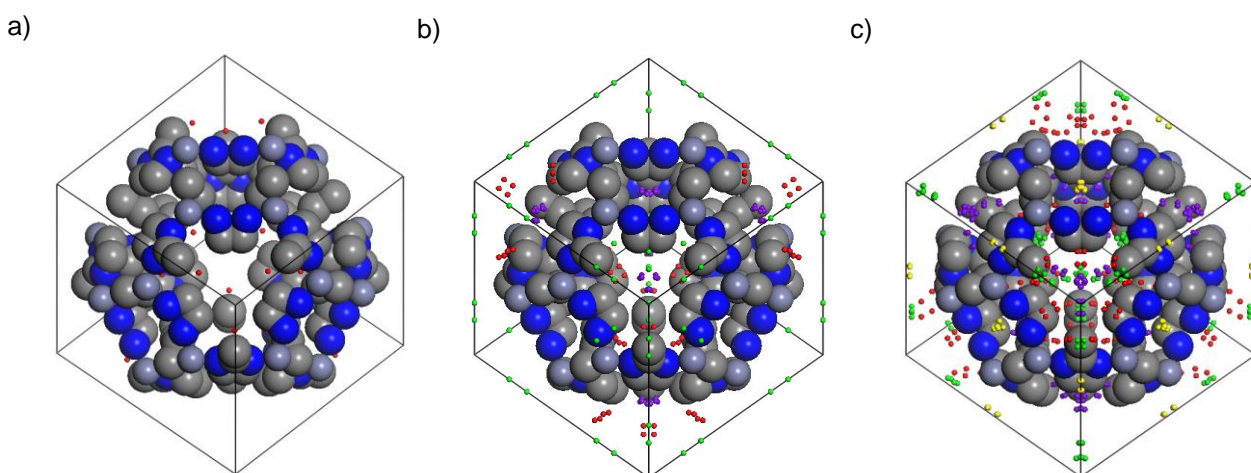


Fig. S8. Adsorption sites of N_2 at 80 K on ZIF-8-98 at **a)** 0.0469 bar; **b)** 0.068 bar; **c)** 1.3486 bar. Grey, carbon atoms; blue, nitrogen atoms; cyan, zinc atoms; red, N_2 molecules adsorbed at site I; purple, N_2 molecules adsorbed at site II; green, N_2 molecules adsorbed at site III; yellow, N_2 molecules adsorbed at site IV.

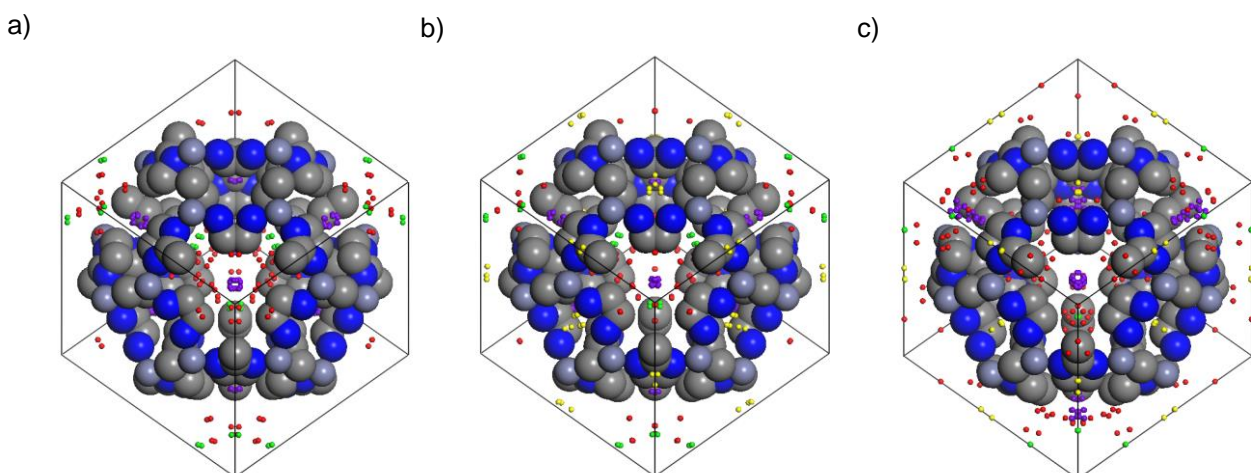


Fig. S9. Adsorption sites of N_2 at 80 K on ZIF-8-0.14 at **a)** 0.0146 bar; **b)** 0.35 bar; **c)** 1.3580 bar. Grey, carbon atoms; blue, nitrogen atoms; cyan, zinc atoms; red, N_2 molecules adsorbed at site I; purple, N_2 molecules adsorbed at site II; green, N_2 molecules adsorbed at site III; yellow, N_2 molecules adsorbed at site IV.

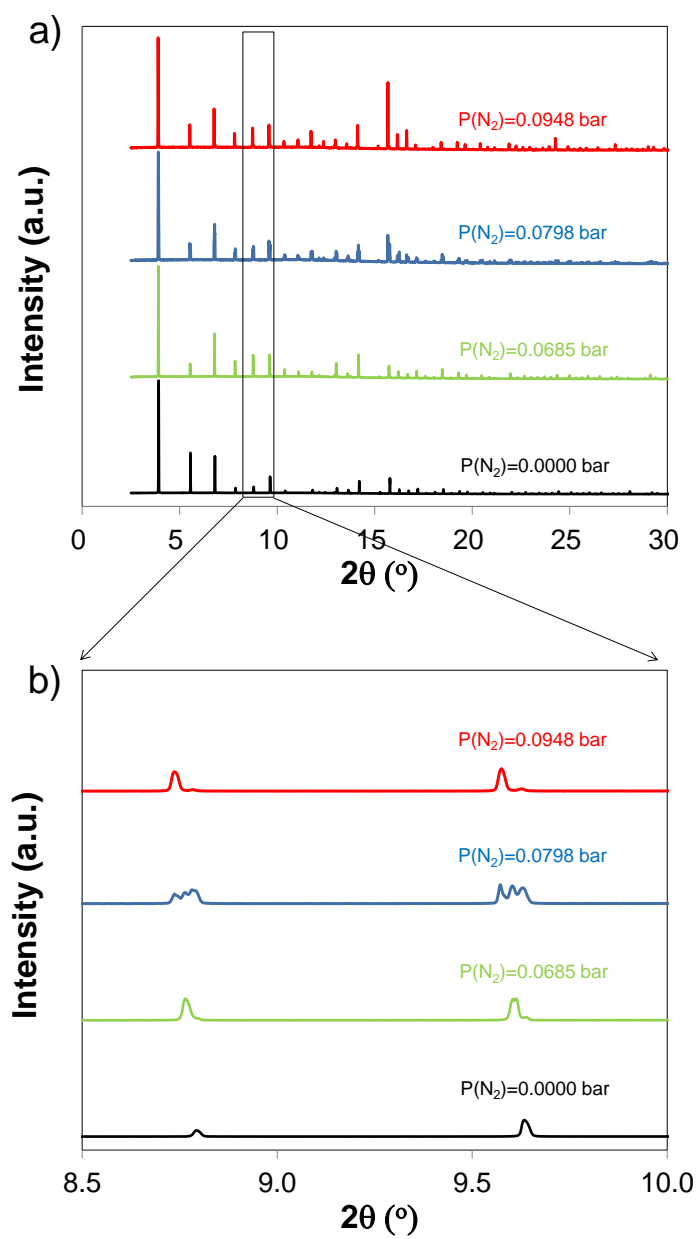


Fig. S9. In situ XRD of ZIF-8-98 at different N_2 pressure.

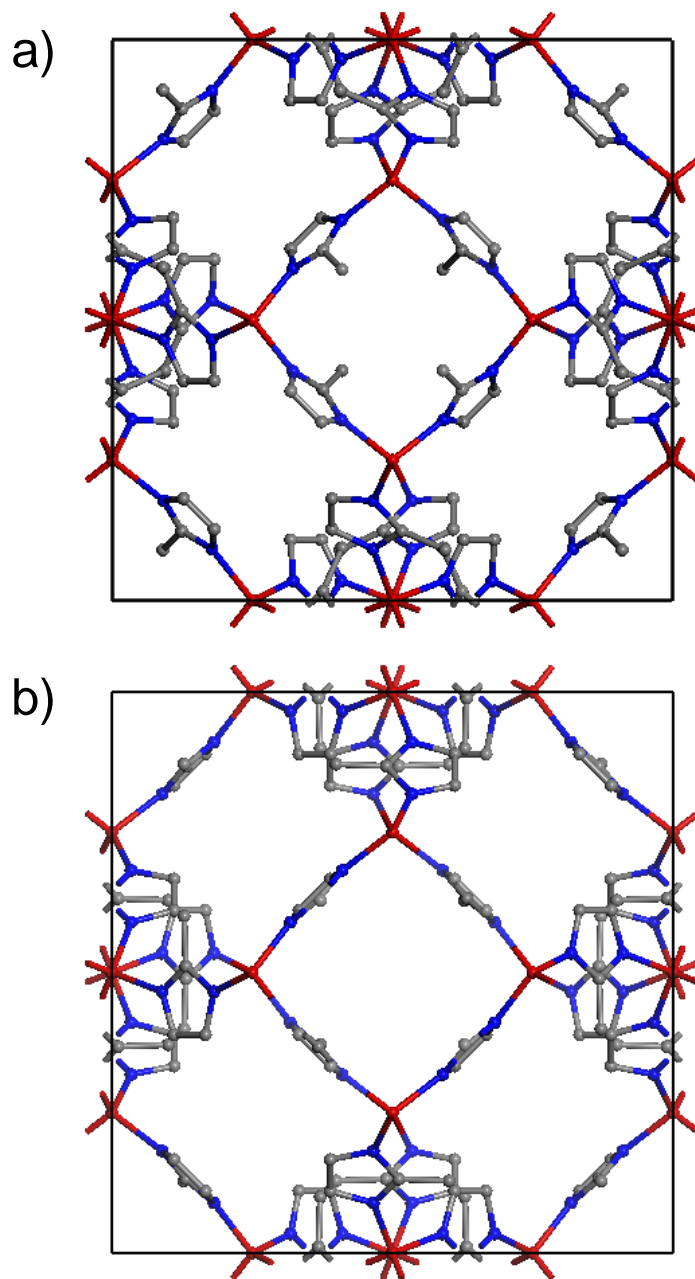


Fig. S10. Unit cell of ZIF-8-98 at a) $p(\text{N}_2) = 0.0000$ bar, b) $p(\text{N}_2) = 1.3468$ bar. Grey spheres, carbon; blue spheres, nitrogen; red spheres, zinc.

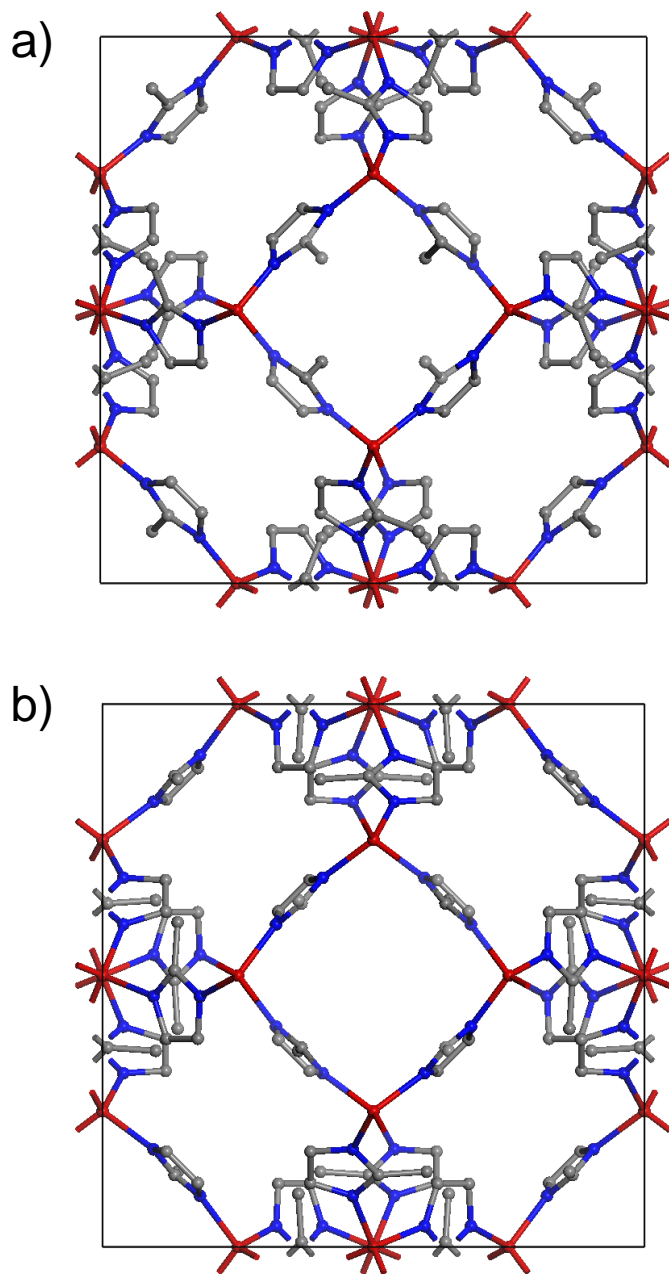


Fig. S11. Unit cell of ZIF-8-0.14 at a) $p(\text{N}_2) = 0.0000$ bar, b) $p(\text{N}_2) = 1.3580$ bar. Grey ball, carbon; blue ball, nitrogen; Red ball, zinc.

S7 References

1. F. Rouquerol, J. Rouquerol, K. S. W. Sing, P. Llewellyn, G. Maurin, Adsorption by powders and porous solids. Academic Press, San Diego, 2nd edn., 2014.
2. C. O. Ania, E. García-Pérez, M. Haro, J. J. Gutiérrez-Sevillano, T. Valdés-Solís, J. B. Parra, and S. Calero, *J. Phys. Chem. Lett.*, 2012, **3**, 1159–1164.1. C. Zhang, J. a. Gee, D. S. Sholl, and R. P. Lively, *J. Phys. Chem. C*, 2014, 140821150523001.
3. J. E. Parker, J. Potter, S. P. Thompson, A. R. Lennie, and C. C. Tang, *Mater. Sci. Forum*, 2012, **706-709**, 1707–1712.
4. S. P. Thompson, J. E. Parker, S. J. Day, A. Evans, and C. C. Tang, *Eur. Astron. Soc. Publ. Ser.*, 2012, **58**, 225–229.
5. S. P. Thompson, J. E. Parker, J. Marchal, J. Potter, A. Birt, F. Yuan, R. D. Fearn, A. R. Lennie, S. R. Street, and C. C. Tang, *J. Synchrotron Radiat.*, 2011, **18**, 637–648.
6. S. P. Thompson, J. E. Parker, J. Potter, T. P. Hill, a. Birt, T. M. Cobb, F. Yuan, and C. C. Tang, *Rev. Sci. Instrum.*, 2009, **80**.
7. E. W. Lemmon, M. O. McLinden, and D. G. Friend, in *NIST Chemistry WebBook*, eds. P. J. Linstrom and W. G. Mallard, National Institute of Standards and Technology, Gaithersburg MD, 20899, USA.
8. A. Coelho, *TOPAS-Academic v5*, Coelho Software, Brisbane, Australia, 2012.
9. S. A. Moggach, T. D. Bennett, and A. K. Cheetham, *Angew. Chemie Int. Ed.*, 2009, **48**, 7087–7089.
10. D. Fairen-Jimenez, S. A. Moggach, M. T. Wharmby, P. A. Wright, S. Parsons, and T. Düren, *J. Am. Chem. Soc.*, 2011, **133**, 8900–8902.